ChemComm

COMMUNICATION

View Article Online
View Journal | View Issue

Cite this: *Chem. Commun.*, 2014, **50**, 3958

Received 12th December 2013,
Accepted 22nd January 2014

DOI: 10.1039/c3cc49454c

www.rsc.org/chemcomm

Sub-5 nm nanobowl gaps electrochemically templated by SiO_2-coated Au nanoparticles as surface-enhanced Raman scattering hot spots†

Haiqiong Wen,[a] Lingyan Meng,[b] Gezhi Kong,[a] Huimin Yu,[a] Zhilin Yang*[b] and Jiawen Hu*[a]

Large-area submonolayer and monolayer Au nanoparticle (NP) arrays with sub-5 nm nanobowl gaps for giant electromagnetic enhancement were created by partially embedding SiO_2-coated Au NP arrays in an electrochemically deposited Au film, followed by the removal of the SiO_2 shells.

In surface-enhanced Raman scattering (SERS), nanometer gap junctions between particles and sharp surface protrusions, known as "hot spots", can create extremely intense local electromagnetic (EM) fields and thus are essential for enormous SERS enhancements.[1,2] For example, recent research revealed that 63 sites of 1 000 000 SERS-active sites contribute 24% of the total SERS intensity.[3] Together with this giant enhancement, the hot spots also result in a very large variation of the SERS signal because for most roughened SERS substrates commonly employed, they are randomly distributed and uncontrollable. This poor spectral reproducibility is one of the main drawbacks that hinder the widespread application of SERS.

Over the past decades, great efforts have been devoted to the construction of hot spots in order to maximize SERS enhancements. Recent achievements and advances include templated NP arrays,[4,5] salt-[6,7] or functional molecule-induced[8,9] NP aggregates, self-assembled NP dimers[10] or arrays,[11] chemically driven NP assembly,[12,13] thermo-sensitive NP assembly,[14] lithography-engineered arrays,[15,16] bilayered Au nanostructures,[17] individual nanometer hole–particle pairs,[18] and mechanically controllable break-junctions.[19] However, the preparation of a SERS substrate with abundant, easy-to-construct, and reproducible nanogaps still remains a great challenge due to complex preparation processes and high cost.

Nanosphere lithography is a well-established technique that utilizes a monolayer colloidal crystal as a lithographic mask to construct structured nanostructures.[20,21] Very recently, we used a polystyrene sphere monolayer to template structured Au sphere segment void (SSV) substrates for the application of borrowed SERS.[22] Inspired by this template idea, here, we further utilize SiO_2-coated Au ($Au@SiO_2$) NP arrays as a template to create reproducible sub-5 nm nanobowl gaps around Au NP arrays. This method allows us to take advantage of routine NP synthesis and electrodeposition techniques to create nanometer sized gaps that are beyond current lithography. Furthermore, the open bowl gaps largely increase the volume of the hot spots, which allows more molecules to be loaded and thereby may generate new spectral characteristics for SERS substrates.

Fig. 1 shows the preparation process of the nanobowl gaps, which involved the assembly of $Au@SiO_2$ NP arrays on a conductive Au surface (denoted as Au substrate hereafter), electrodeposition of Au, and removal of the SiO_2 shells. The synthesis of $Au@SiO_2$ NPs, with 55 nm Au cores and <5 nm thick SiO_2 shells, was performed following a reported method.[23,24] After synthesis, cyclic voltammetry and SERS tests were performed to diagnose the pinholes on the shell of the $Au@SiO_2$ NPs.[24] Only pinhole-free $Au@SiO_2$ NPs that show no Au oxide stripping peak and no SERS peaks (Fig. S2 and S3, ESI†) were chosen. Such an examination and the insulated nature of SiO_2 ensure that the Au deposit film grows around, instead of covers, the $Au@SiO_2$ template NPs during the following electrodeposition.

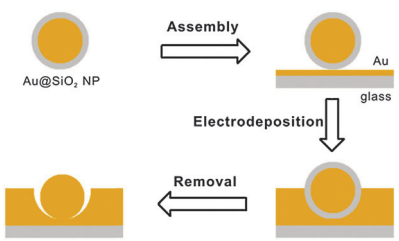

Fig. 1 Schematic illustration of the preparation flow of the Au NP arrays surrounded with sub-5 nm nanobowl gaps.

[a] *State Key Laboratory for Chemo/Biosensing and Chemometrics, and College of Chemistry and Chemical Engineering, Hunan University, Changsha, 410082, China. E-mail: jwhu@hnu.edu.cn; Fax: +86-731-85956121*

[b] *Department of Physics, Xiamen University, Xiamen 361005, China. E-mail: zlyang@xmu.edu.cn*

† Electronic supplementary information (ESI) available: Experimental section, details for the 3D-FDTD simulations and evaluation of the enhancement factor, and supplementary results of UV-Vis, CV, SEM, 3D-FDTD simulations, and SERS spectra. See DOI: 10.1039/c3cc49454c

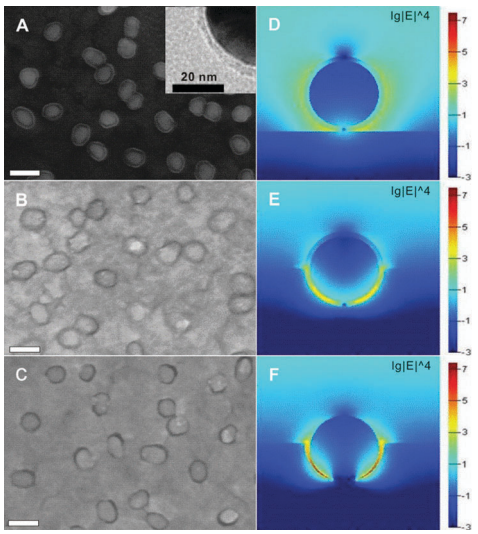

Fig. 2 SEM images (A–C) and corresponding EM field distribution images (D–F) of submonolayer Au@SiO_2 NP arrays on an Au surface before electrodeposition (A and D), after electrodeposition of a 32 nm-thick Au film (B and E), and upon removal of the silica shells (C and F). The inset in image A is a magnified TEM image showing the shell of a Au@SiO_2 NP. Scale bars are 100 nm.

Submonolayer Au@SiO_2 NP arrays were assembled on the Au substrate by immersing a 3-aminopropyltrimethoxysilane (APTS)-functionalized substrate in the Au@SiO_2 aqueous solution; whilst monolayer Au@SiO_2 NP arrays were first assembled at a water–air interface followed by transferring them onto the Au substrate (the preparation processes for both arrays are detailed in the ESI†). Fig. 2A and Fig. S4A, ESI† show SEM images of the submonolayer and monolayer Au@SiO_2 NP arrays assembled on the Au substrate, respectively. In the submonolayer arrays, the Au@SiO_2 NPs are randomly distributed with each particle encircled by a clear light layer of about 4 nm thickness, *i.e.*, the SiO_2 shell. In contrast, the Au@SiO_2 NPs are closely packed in the monolayer arrays. Au was deposited through the Au@SiO_2 NP arrays using a commercial Au plating solution TSG-250 at a constant current of 10 μA cm^{-2}. A 32 nm thick Au film was deposited by monitoring the charge passed during electrodeposition and employing 70% efficiency for the electrodeposition. Fig. 2B and Fig. S4B, ESI† show that the surface of the electrochemically deposited Au film is smooth, in which the Au@SiO_2 NPs are, as expected, partially embedded. Successful template construction of the nanobowl gaps requires the Au deposit film to be thinner than the diameter of the template NPs and be as smooth as possible. However, at such a small thickness, the surface roughness of the underneath Au substrate, which was prepared by vacuum evaporation, would unavoidably be transferred to the thin Au film deposited. We originally used a home-made Au plating solution, but only achieved a rough, non-uniform Au deposit film. It is known from electrodeposition science that a plating solution added with special additives has an excellent throwing power and levelling effect, *i.e.*, an ability to deposit metals uniformly and a natural ability to level the imperfections on an irregular surface. After trying a few commercial Au plating solutions, we found that TSG-250 allows us to achieve the desired smooth, flat Au deposit film.

Following electrodeposition, the SiO_2 shell was removed by dissolving the SiO_2 shell in a 5 M NaOH solution. The higher magnification SEM images, shown in Fig. 2C and Fig. S4C, ESI,† clearly reveal that a nanobowl gap is created around each particle in the arrays. To further demonstrate the successful creation, Fig. S5, ESI† shows lower magnification SEM images of both submonolayer and monolayer arrays before and after the removal of the SiO_2 shell. The smooth surface of the Au deposit film is retained after the removal of the SiO_2 shell under severe alkaline conditions, thereby largely restraining the contributions coming from a non-uniform surface morphology, beside the desired nanobowl gaps, to the observed SERS intensity. For the templated gaps, their resolution in *x*- and *y*-directions is determined by the shell size of the Au@SiO_2 NPs, thereby achieving a nanometer resolution because the present NP synthesis techniques allow control of the NP size with nanometer precision. The resolution in the *z*-direction is determined by the height of the deposit, which could even achieve an atomic layer precision if an atomic layer deposition technique, *e.g.*, underpotential deposition,[25] was used. Ideally, a deposited film with a flat surface finish and precisely controlled thickness is highly desired for the preparation of templated nanogaps with high resolution.

To establish the SERS behaviour of the Au NP arrays surrounded with sub-5 nm nanobowl gaps, 4-mercaptobenzoic acid (4-MBA) was used as a probe molecule, which was adsorbed on the arrays by immersing the arrays in a 1 mM 4-MBA solution in ethanol for 30 minutes. Fig. 3 and Fig. S6, ESI† show that the SERS intensities are negligible for the exposed submonolayer and monolayer Au@SiO_2 NP arrays. After partially embedding the arrays in the Au deposit film, the SERS intensities for the two Au NP arrays surrounded with sub-5 nm nanobowl gaps are much stronger, about 7 times stronger than the corresponding arrays without the gaps, thereby confirming a 85% contribution from the gaps created. The strong SERS peaks at 1077 and 1587 cm^{-1} are assigned to the ν_{12} and ν_{8a} vibration modes of the aromatic ring, respectively;[26] whilst the other three moderately strong peaks at 689, 998, and 1020 cm^{-1} are characteristic of monosubstituted benzene derivatives.[27] For the submonolayer and monolayer arrays surrounded with the sub-5 nm

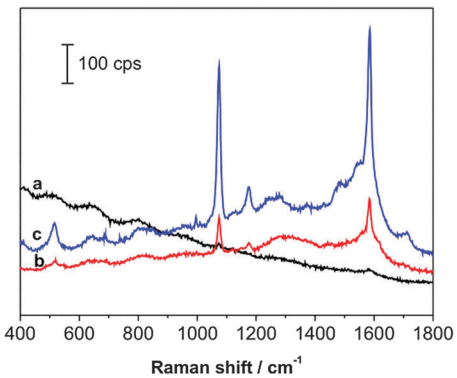

Fig. 3 SERS spectra of 4-MBA adsorbed submonolayer Au@SiO_2 NP arrays before electrodeposition (a), after electrodeposition of a 32 nm-thick Au film (b), and upon removal of the silica shells (c). Excitation line: 632.8 nm; accumulation time: 10 s. To avoid the laser burning the molecule, its intensity is attenuated to an extent that the intensity of the 520 cm^{-1} peak of silicon for a 1 s accumulation is 423 cps.

nanobowl gaps, their averaged enhancement factors are estimated to be 2.5×10^5 and 1.94×10^5, respectively (for details, see ESI†). To further reveal the regional intensity variation, SERS measurements were taken across the two arrays 20 times. Fig. S7 and S8, ESI† indicate that the spectral variations on the two arrays are less than 17.3% and 5.2%, respectively. As the two arrays have no structured surfaces, their unexpected good spectral reproducibility can only be attributed to a large increase in hot spot density (or hot spot volume), which averages out the variation in SERS intensity and thus improves spectral reproducibility.

The EM fields generated by the related nanostructured surfaces are inherent to the SERS behaviours observed above. To quantitatively understand the SERS behaviours, theoretical simulations were performed using a three-dimensional finite-difference time-domain (3D-FDTD) method, as detailed in the ESI.† To conveniently determine the order of enhancement and find the location of the hot spots, near field enhancement distributions of $|E|^4$ are shown under logarithmic coordinates and are normalized by the fourth power of the electric field of the incident wave at the position of the molecule. The enhancement factor for SERS is proportional to E^4, where E represents the field enhancement defined as the ratio of the local field E_{loc} to the incoming field E_{in}, $E = |E_{loc}|/|E_{in}|$. Before electrodeposition, the Au@SiO_2 NP arrays were exposed on the supporting Au substrate. The hot spots are located at the junctions between the Au@SiO_2 NPs and the bottom Au substrate (Fig. 2D and Fig. S4D, ESI†), where the enhancement factors achieve maximum values of 2.5×10^3 and 3.2×10^4 for the submonolayer and monolayer Au@SiO_2 NP arrays, respectively. Molecules placed in these hot spots would experience SERS enhancement, known as shell-isolated nanoparticle-enhanced Raman spectroscopy established by the Tian group in 2010.[24] In our case, the 4-MBA molecules were hindered to enter the hot spots by the APTS layer, which was adsorbed on the Au substrate to anchor the Au@SiO_2 NPs and isolated from the Au core by the pinhole-free SiO_2 shell, so that the SERS peaks are rather weak (curve a in Fig. 3 and Fig. S6, ESI†). After electrodeposition, the Au@SiO_2 NP arrays were partially embedded in the Au deposit film. In this case, the hot spots are located in the silica layer between the Au NPs and the Au deposit film (Fig. 2E and Fig. S4E, ESI†), and the maximum enhancement factors reach 4.0×10^4 and 1.6×10^4 for the submonolayer and monolayer Au@SiO_2 NP arrays, respectively. As the hot spots are inaccessible for the probe molecules, the weak SERS signals (curve b in Fig. 3 and Fig. S6, ESI†) should be attributed to the imperfections on the Au deposit film, which are unable to be eliminated completely even using a high quality commercial Au plating solution. Upon removal of the SiO_2 shell, the enhanced EM field is concentrated in the nanobowl gap particularly at its bottom. The calculated maximum SERS enhancements for the submonolayer and monolayer Au NP arrays are as high as 2.5×10^7 and 1.0×10^6, respectively, which are 1–2 orders of magnitude larger than the enhancements obtained in the experimental systems. Considering that the surface averaged SERS enhancement is often 1–2 orders of magnitude lower than the maximum value,[3,28] the calculated EFs are thus in good agreement with the EFs experimentally determined because the latter are the averaged EFs over the entire surface. To directly choose NPs that are able to template nanobowl gaps with giant EM fields, theoretical simulations were further performed for a series of nanobowl gaps made from arrays with different shell thicknesses. Fig. S9, ESI† shows that when the shell thickness decreases from 4 to 3, 2, and 1 nm, the maximum enhancement factor for the templated nanobowl gaps gradually decreases from 2.5×10^7 to 1.0×10^7, 1.3×10^6, and 2.0×10^5, respectively. Therefore, Au@SiO_2 NPs with 4 nm shells are the best choice among the four sorts of Au@SiO_2 NPs examined for templating the nanobowl gaps.

In summary, we templated sub-5 nm nanobowl gaps around Au@SiO_2 NPs with <5 nm shells, taking advantage of NP synthesis and electrodeposition techniques. Compared to the small exterior ''hot spots'' between adjacent NPs, the open nanobowl gaps do not just produce giant EM enhancements. They also largely increase the volume for the hot spots to load a higher amount of Raman dyes, thereby averaging out the large signal variation commonly observed on a disordered SERS substrate. The method described here opens avenues for the creation of gaps of only a few nanometers using routine laboratory techniques, which may find widespread applications in SERS and other fields, *e.g.*, molecular electronics.

This work was financially supported by the National Natural Science Foundation of China (Grant No. 20873037, 91027037, J1103312, J1210040, 21173171, and 11074210).

Notes and references

1 H. Xu, J. Aizpurua, M. Käll and P. Apell, *Phys. Rev. E*, 2000, **62**, 4318.
2 H. Xu, E. J. Bjerneld, M. Käll and L. Börjesson, *Phys. Rev. Lett.*, 1999, **83**, 4357.
3 Y. Fang, N.-H. Seong and D. D. Dlott, *Science*, 2008, **321**, 388.
4 P. Nielsen, S. Hassing, O. Albrektsen, S. Foghmoes and P. Morgen, *J. Phys. Chem. C*, 2009, **113**, 14165.
5 H. H. Wang, C. Y. Liu, S. B. Wu, N. W. Liu, C. Y. Peng, T. H. Chan, C. F. Hsu, J. K. Wang and Y. L. Wang, *Adv. Mater.*, 2006, **18**, 491.
6 J. Chen, B. Shen, G. Qin, X. Hu, L. Qian, Z. Wang, S. Li, Y. Ren and L. Zuo, *J. Phys. Chem. C*, 2012, **116**, 3320.
7 W. Li, P. H. C. Camargo, X. Lu and Y. Xia, *Nano Lett.*, 2009, **9**, 485.
8 D.-K. Lim, K.-S. Jeon, H. M. Kim, J.-M. Nam and Y. D. Suh, *Nat. Mater.*, 2009, **9**, 60.
9 M. M. Maye, D. Nykypanchuk, M. Cuisinier, D. van der Lelie and O. Gang, *Nat. Mater.*, 2009, **8**, 388.
10 H. Guo, D. Jiang, H. Li, S. Xu and W. Xu, *J. Phys. Chem. C*, 2013, **117**, 564.
11 H. Wang, C. S. Levin and N. J. Halas, *J. Am. Chem. Soc.*, 2005, **127**, 14992.
12 G. Braun, I. Pavel, A. R. Morrill, D. S. Seferos, G. C. Bazan, N. O. Reich and M. Moskovits, *J. Am. Chem. Soc.*, 2007, **129**, 7760.
13 G. Chen, Y. Wang, M. Yang, J. Xu, S. J. Goh, M. Pan and H. Chen, *J. Am. Chem. Soc.*, 2010, **132**, 3644.
14 Y. Wu, F. Zhou, L. Yang and J. Liu, *Chem. Commun.*, 2013, **49**, 5025.
15 H. Duan, H. Hu, H. K. Hui, Z. Shen and J. K. Yang, *Nanotechnology*, 2013, **24**, 185301.
16 H. Im, K. C. Bantz, S. H. Lee, T. W. Johnson, C. L. Haynes and S.-H. Oh, *Adv. Mater.*, 2013, **25**, 2678.
17 D.-K. Lim, K.-S. Jeon, J.-H. Hwang, H. Kim, S. Kwon, Y. D. Suh and J.-M. Nam, *Nat. Nanotechnol.*, 2011, **6**, 452.
18 H. Wei, U. Håkanson, Z. Yang, F. Höök and H. Xu, *Small*, 2008, **4**, 1296.
19 J.-H. Tian, B. Liu, X.-L. Li, Z.-L. Yang, B. Ren, S.-T. Wu, N.-J. Tao and Z.-Q. Tian, *J. Am. Chem. Soc.*, 2006, **128**, 14748.
20 K. A. Willets and R. P. Van Duyne, *Annu. Rev. Phys. Chem.*, 2007, **58**, 267.
21 S. Cintra, M. E. Abdelsalam, P. N. Bartlett, J. J. Baumberg, T. A. Kelf, Y. Sugawara and A. E. Russell, *Faraday Discuss.*, 2006, **132**, 191.
22 J. Hu, S. Chen, R. P. Johnson, X. Lin, Z. Yang and A. E. Russell, *J. Phys. Chem. C*, 2013, **117**, 24843.

23 L. M. Liz-Marzán, M. Giersig and P. Mulvaney, *Langmuir*, 1996, **12**, 4329.
24 J. F. Li, Y. F. Huang, Y. Ding, Z. L. Yang, S. B. Li, X. S. Zhou, F. R. Fan, W. Zhang, Z. Y. Zhou, D. Y. Wu, B. Ren, Z. L. Wang and Z. Q. Tian, *Nature*, 2010, **464**, 392.
25 E. Herrero, L. J. Buller and H. D. Abruña, *Chem. Rev.*, 2001, **101**, 1897.
26 H. Park, S. B. Lee, K. Kim and M. S. Kim, *J. Phys. Chem.*, 1990, **94**, 7576.
27 F. R. Dollish, W. G. Fateley and F. F. Bentley, *Characteristic Raman frequencies of organic compounds*, Wiley, New York, 1974, pp. 162–190.
28 S. L. Kleinman, R. R. Frontiera, A.-I. Henry, J. A. Dieringer and R. P. Van Duyne, *Phys. Chem. Chem. Phys.*, 2013, **15**, 21.